Earth and Planetary Science Letters 274 (2008) 241–249

Contents lists available at ScienceDirect

Earth and Planetary Science Letters

journal homepage: www.elsevier.com/locate/epsl

Thermodynamics of SiO_2–H_2O fluid near the upper critical end point from quartz solubility measurements at 10 kbar

Robert C. Newton, Craig E. Manning *

Department of Earth and Space Sciences, University of California, Los Angeles, CA 90095, USA

ARTICLE INFO

Article history:
Received 5 May 2008
Accepted 22 July 2008
Available online 30 August 2008

Editor: L. Stixrude

Keywords:
supercritical fluids
hydrous melting
quartz solubility
experimental petrology

ABSTRACT

Quartz solubility in SiO_2–H_2O fluid was measured at 10 kbar and 750–1130 °C in a piston-cylinder apparatus. At ≤1035 °C, solubility was determined by weight loss of single crystals equilibrated with H_2O-rich fluid; at higher temperature (T), the fluid phase coexisting with quartz quenched to a glass, and solubility was determined by phase-assemblage bracketing (quartz present or absent with glass in quenched charges). At 700 to 1000 °C, quartz solubility increases at an accelerating rate from 1.2 mol% to 8.9 mol% SiO_2. Above 1000 °C, there is a sharp increase to nearly equimolar fluids in equilibrium with quartz at 1080 °C. At T>1080 °C, SiO_2 concentration increases less strongly. The data confirm the existence of a critical end point on the hydrous melting curve of quartz, and imply it lies at 1080 °C and 9.5–10 kbar. Two independent approaches to calculating SiO_2 activity at 1080 °C — from a mixing model for aqueous SiO_2 extrapolated from lower temperatures, and from depression of the melting temperature of quartz by H_2O — indicate nearly constant values over the wide compositional range of 20–60 mol% SiO_2. The activity of H_2O (a_h) at the same conditions, calculated by integration of the Gibbs–Duhem relation, shows a plateau of very high a_h (~0.93) in the same broad composition range. At ≥60 mol%, there is an abrupt change in H_2O dissolution mechanism, as SiO_2 activity becomes proportional to its mole fraction at high silica concentration. The activity-concentration relations at 1080 °C and 10 kbar were fitted to a subregular solution model, giving interchange energies for SiO_2 and H_2O of respectively 25.3 and 14.3 kJ/mol. Roughly constant SiO_2 activity of the near-critical fluid despite a factor of 3 increase in X_{H2O} can be explained by progressively greater amounts of hydrogen bonding of H_2O molecules to polymerized silica units, so that the effective concentration of these units remains nearly constant as H_2O increases. The sudden onset of critical phenomena in the system SiO_2–H_2O as temperature and pressure increase over narrow intervals approaching 1080 °C and 10 kbar is thus explained as mainly a convergent or cooperative compositional effect, in which polymerization and hydrogen bonding both play important roles.

1. Introduction

The tendency of hydrous silicate magmas to become fully miscible with an H_2O-rich vapor phase at high pressure (P) and temperature (T) has fundamental implications for fluid-rock interaction in the lower crust and upper mantle (Manning, 2004; Hack et al., 2007a,b). Because silicates have low volatility and are sparingly soluble in H_2O, rock-H_2O systems may exhibit critical end points on their hydrous melting curves (e.g., Hack et al., 2007a). The critical behavior of several geologically relevant model compositions have now been investigated (e.g., Kennedy et al., 1962; Shen and Keppler, 1997; Bureau and Keppler, 1999; Stalder et al., 2000; Sowerby and Keppler, 2002; Kessel et al., 2005a,b; Mibe et al., 2007; Hermann and Spandler, 2008). At pressures in excess of the upper critical end points of such systems, supercritical multicomponent fluids are extremely mobile (Audétat and Keppler, 2004), and may be important metasomatic agents in subduction zones and other high-pressure environments.

Although there has been significant effort devoted to establishing the locations of critical end points in model systems, the thermodynamic properties of the supercritical silicate-H_2O mixtures remain poorly known (e.g., Hack et al., 2007b). Because SiO_2 is the most abundant rock-forming oxide, the key binary system for which to determine thermodynamic properties of the supercritical mixture is SiO_2–H_2O. To constrain the mixing properties of supercritical SiO_2–H_2O, we conducted experiments on quartz solubility in H_2O from 750–1130 °C at 10 kbar. The results confirm the existence of a high-T critical end point in the system, provide data that constrain activity-composition relations of supercritical quartz-saturated SiO_2–H_2O fluids, and yield insights into speciation of SiO_2 near the critical end point.

* Corresponding author.
E-mail address: manning@ess.ucla.edu (C.E. Manning).

0012-821X/$ – see front matter © 2008 Elsevier B.V. All rights reserved.
doi:10.1016/j.epsl.2008.07.028

2. Background to the system SiO_2–H_2O

2.1. Phase equilibria

Quartz has low solubility at low T and P near the critical point of H_2O, as shown by many early experimental studies (Kennedy, 1950; Morey and Hesselgesser, 1951; Wyart and Sabatier, 1955). The modest SiO_2 content of aqueous fluid at these conditions is not sufficient to produce a large shift of the critical point of H_2O; accordingly, a quartz-saturated critical end point exists in the system SiO_2–H_2O which is only slightly removed from the critical T and P of pure H_2O. However, at higher P and T, quartz becomes much more soluble. For example, at 2 kbar H_2O pressure and 800 °C, quartz is nearly 100 times more soluble than at the critical point of H_2O (Anderson and Burnham, 1965). Raising pressure at high T further increases quartz solubility (Anderson and Burnham, 1965; Manning, 1994). Because of the marked depression of the melting point of quartz with increasing P_{H_2O}, the constitution of a SiO_2-rich aqueous fluid and of a hydrous silica melt in equilibrium with quartz may become coincident and indistinguishable at an upper critical end point (UCEP), with consequent termination of the three-phase equilibrium quartz-aqueous fluid-melt (Fig. 1). A discrete vapor-saturated melting point of quartz does not exist at pressures above the UCEP, but rather a continuum of solutions progressively richer in SiO_2 in equilibrium with quartz as temperature increases.

Kennedy et al. (1962) measured the aqueous solubility of quartz and the depression of the melting point by H_2O at pressures to 9.5 kbar. They found a convergence of the compositions of co-existing aqueous and siliceous fluids with increasing pressure along the hydrous melting curve, and proposed a UCEP at 9.7 kbar and 1080 °C (Fig. 2). Kennedy et al. (1962) found that the composition of the critical fluid in equilibrium with quartz is close to equimolar SiO_2 and H_2O. The existence of a UCEP was challenged by Stewart (1967) and Mysen (1998), but several synthesis brackets of quartz saturation by Nakamura (1974) imply that the system is super-critical at 15 kbar, and therefore that the UCEP exists at lower P. Thus, the location, and perhaps even the existence, of a UCEP in the system SiO_2–H_2O remains uncertain.

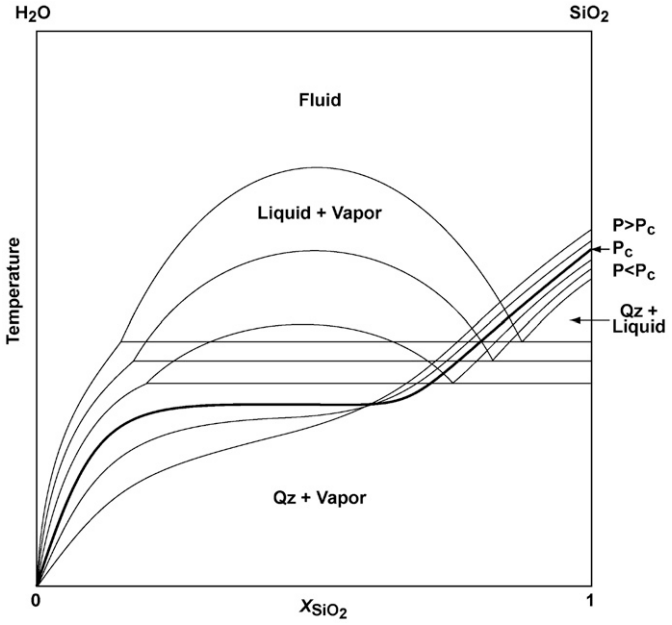

Fig. 1. Schematic isobaric T–X sections of fluid compositions in the system SiO_2–H_2O. P_c denotes the pressure of a critical end point on the vapor-saturated melting curve of quartz. Vapor and liquid refer, respectively, to coexisting H_2O-rich and SiO_2-rich compositions.

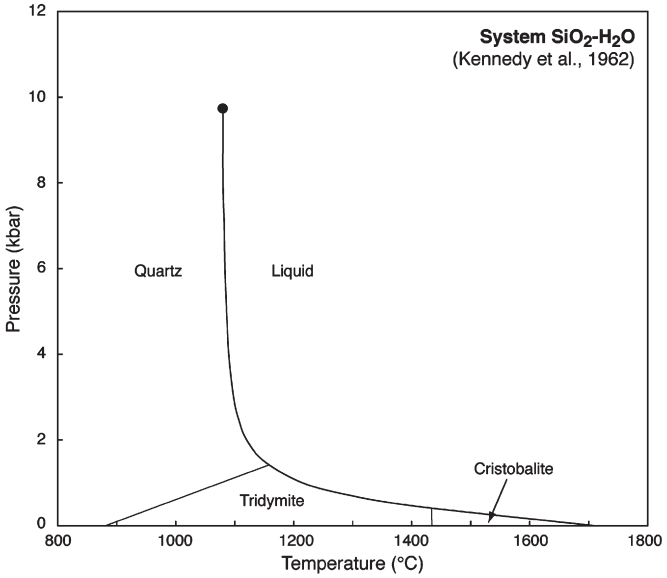

Fig. 2. Vapor-saturated melting curve of quartz in the system SiO_2–H_2O according to Kennedy et al. (1962). They show a high-pressure critical end point on the melting curve near 10 kbar and 1080 °C.

2.2. Speciation in SiO_2–H_2O fluids

Thermodynamic analysis of quartz solubility data suggests that the major species of solute silica at elevated T and pressures of several kilobars is the monomer $Si(OH)_4 \cdot (n-2)H_2O$, where n is the total hydration number, and $n-2$ is the number of hydrogen-bonded H_2O molecules per Si (Wasserburg, 1957; Weill and Fyfe, 1964; Sommerfeld, 1967). Analysis of quartz solubility in CO_2–H_2O and Ar–H_2O solutions at elevated T and P led Walther and Orville (1983) to conclude that n is 3 to 5; that is, $Si(OH)_4$ units are hydrogen-bonded with one to three additional H_2O molecules. Newton and Manning (2000), by a similar analysis of quartz solubility in CO_2–H_2O at higher T and P (800 °C, 10 kbar), found that n could be as high as five and may decrease with decreasing H_2O activity.

Existence of the monomeric silica species was confirmed by Raman spectroscopy at high P and T by Zotov and Keppler (2000), who also found evidence for an abundant additional species, the dimer $Si_2O(OH)_6 \cdot (2k-3)H_2O$, where the total hydration number k per SiO_2 unit need not be the same as n for the monomer. The relative concentration of the dimer increases with both T and P (Zotov and Keppler, 2000, 2002). Because increases in T and P also yield greater quartz solubility, it can further be concluded that the proportion of dimers increases with total silica concentration.

Independent evidence for the existence of the dimer at high SiO_2 concentration comes from the phase-equilibrium investigation of Zhang and Frantz (2000) in the system MgO–SiO_2–H_2O at 10–20 kbar and 900–1200 °C. They determined the SiO_2 concentration of aqueous fluid in equilibrium with enstatite and forsterite by a phase boundary projection method. The measured silica concentrations were lower than expected on the basis of ideal-solution models of silica monomers and H_2O. Zhang and Frantz (2000) therefore suggested that substantial amounts of a dimeric species might be present at their experimental P–T conditions, resulting in negative deviations from ideal solution. Newton and Manning (2002) confirmed the relatively low activity of solute SiO_2 by direct measurement of enstatite + forsterite solubility at high T and P using a weight-loss method.

Newton and Manning (2002) and Zotov and Keppler (2002) independently proposed and calibrated a simple model for SiO_2 speciation based on concentrations measured by weight-loss experiments and by Raman spectroscopy, respectively. Following Newton

and Manning (2002), homogeneous equilibrium between monomers and dimers can be written, neglecting H_2O solvation, as

$$\underset{\text{monomer}}{2Si(OH)_4} = \underset{\text{dimer}}{Si_2O(OH)_6} + H_2O \quad (1)$$

for which the equilibrium constant (K_1) at constant T and P is

$$K_1 = \frac{a_d a_h}{a_m^2} \quad (2)$$

where a is activity and the subscripts m, d and h indicate respectively monomer, dimer, and H_2O. By choosing a standard state for total dissolved SiO_2 ($SiO_{2,aq}$) of unit activity of the hypothetical solution with unit mole fraction of monomers (X_m), referred to infinite dilution, and assuming ideal mixing of solute species, Newton and Manning (2002) showed that Eq. (2) can be written in terms of the mole fraction of total dissolved silica (X_s) as

$$K_1 = \frac{1-\gamma_{s,s}}{2\gamma_{s,s}^2 X_s} \quad (3)$$

where $\gamma_{s,s}$ is the activity coefficient of $SiO_{2,aq}$ on this "solute" standard state and SiO_2 concentration is ≤2 molal, so that a_h can be assumed to be unity. Newton and Manning (2002, 2003) showed that $\gamma_{s,s}$ may be retrieved from measurements of quartz solubility, according to the dissolution reaction:

$$\underset{\text{quartz}}{SiO_2} = SiO_{2,aq} \quad (4)$$

coupled with measurements of SiO_2 solubility of another silica-buffering assemblage such as enstatite–forsterite:

$$\underset{\text{enstatite}}{2MgSiO_3} = \underset{\text{forsterite}}{Mg_2SiO_4} + SiO_{2,aq} \quad (5)$$

Their calibration of K_1 based on enstatite–forsterite solubility measurements in the range 600–900 °C and 4–14 kbar, is in very good agreement with the spectroscopic calibration of Zotov and Keppler (2002) in the same P–T range.

Although the above formulation gives a good account of silica activity and speciation in the relatively dilute concentration range below about 2 molal, it is clearly not applicable to the higher concentrations encountered as T and P increase toward the proposed critical end point. At near-critical compositions the silica likely forms additional species, such as and chain oligomers, or more polymerized sheets and three-dimensional clusters. Moreover, the H_2O activity cannot be assumed to be unity in such concentrated solutions. Finally, the polymer hydration states, which include both hydroxyl and hydrogen-bonded H_2O according to some partitioning law, are completely unknown for complexly polymerized silica.

2.3. Equations of state

Manning (1994) extended the data set of quartz solubility in H_2O to 900 °C and 20 kbar. He found that these new data and all of the existing data at lower T and P could be systematized by a correlation of log SiO_2 molality with log H_2O density to produce a comprehensive formula for quartz solubility over a great range of T and P. He restricted his expression to <900 °C because of the rapid increase of solubility at higher T approaching the upper critical end point. Manning's (1994) formula does not account for SiO_2 activity or speciation.

Gerya et al. (2005) took polymerization into account in deriving a quartz solubility formula similar to that of Manning (1994). They utilized a dimer formation constant analogous to K_1 and envisioned subsequent attachments of SiO_4^{4-} groups to form longer chains, with successive attachment reactions governed by the same equilibrium constant. Their formula is quite successful in describing the solubility data over the same P–T range as treated by Manning (1994), but does not consider polymers other than long chains, takes no account of hydrogen-bonded H_2O, and does not provide for a critical end point.

2.4. Outstanding problems and scope of the present work

Fundamental problems remain concerning the melting and solubility of quartz in the region of the presumed UCEP. The UCEP was only approximately located by Kennedy et al. (1962), at conditions beyond the range of their experiments. Although Nakamura's (1974) data nominally provide an upper pressure limit of 15 kbar on a critical end point in the system, experiments on more complex compositional systems have been interpreted to preclude a UCEP in SiO_2–H_2O (Stewart, 1967; Mysen, 1998). In addition, the UCEP position and hydrous melting curve proposed by Kennedy et al. (1962) is problematic. They noted that, according to their measurements, the H_2O content of the melt increases greatly in the range 4–10 kbar, approaching the UCEP pressure, yet the melting temperature decreases only slightly over this pressure interval, from 1095 to 1080 °C. This is quite unlike the hydrous melting behavior of silicate minerals such as albite in the same pressure range (Burnham and Davis, 1974). An approximate "lattice gas" analysis of H_2O–SiO_2 fluid mixtures by Kennedy et al. (1962) suggested that, at pressures approaching the proposed UCEP, where the melt becomes very hydrous, depression of the melting point should be much more pronounced. Kennedy et al. (1962) noted that the critical composition near X_s=0.5 could correspond to a regular solution (Guggenheim, 1952), yet the sudden onset of critical mixing over only a few tens of degrees and one kbar could not be modeled by any such simple solution model, nor would such a model be adequate for a system having the extensive polymerization expected of SiO_2-rich fluids.

These uncertainties motivated a reinvestigation of the system SiO_2–H_2O in the P–T–X range near the proposed UCEP. The experiments address the outstanding problems identified above, as well as experimental issues that may have led to problems in the Kennedy et al. (1962) study. For example, the Kennedy et al. (1962) melting experiments were only a few minutes in duration, so it is possible that they metastably overstepped the true equilibrium melting points in the high pressure region. In addition, there could have been difficulty in recognizing the start of melting near the critical point because aqueous fluid quenched from this region yields a glassy siliceous gel which may be hard to distinguish from a quenched melt phase. The most straightforward way to circumvent these potential problems is to measure, to high accuracy and precision, the isobaric variation in the solubility of quartz over a large range near the proposed critical pressure. This approach is advantageous because the shapes of isobaric solubility curves provide definitive evidence for the presence or absence of a critical end point, and, if of sufficient accuracy, can be modeled to obtain activity–composition relations, which, in turn, could give some insight into solute speciation and polymerization behavior in concentrated SiO_2 solutions.

3. Experimental methods

The wide solubility range of this study necessitated two types of experiments: single-crystal solubility runs at low SiO_2 concentration (Q_1 experiments, Table 1), and phase-assemblage bracketing runs at high SiO_2 concentration (Q_2 experiments, Table 1). In Q_1 experiments, starting materials were ultrapure H_2O and a large natural quartz crystal from Brazil (Manning, 1994). Fragments broken from the crystal were shaped into ellipsoids with a diamond file, smoothed with 600-mesh Al_2O_3 paper, and polished with 15-μm diamond paper. A crystal and 10–37 mg of H_2O were sealed by arc-welding in a 1 cm-long length of Pt tubing of 3.5 mm O.D. and 0.15 mm wall thickness,

Table 1
Experimental results at 10 kbar

Run	Type	T (°C)	Time (h)	H_2O in (mg)	Quartz in (mg)	Quartz out (mg)	X_s
14	Q_1, R	750	90	35.656	7.599	5.641	0.0162
1	Q_2, R	950	1.5	26.456	8.807	q	<0.0908
2	Q_1, R	950	2.5	24.616	5.887	0.876	0.0575
5	Q_1, BN	950	3.5	30.438	8.444	2.602	0.0544
3	Q_1, BN	1000	1.7	24.816	11.857	3.822	0.0885
4	Q_1, BN	1035	1	29.786	23.98	8.087	0.1379
6A	Q_2, BN	1050	1.7	2.426	2.375	q	<0.2269
6B	Q_2, BN	1050	1.7	3.147	2.144	–	>0.1696
13	Q_2, BN	1050	3	23.508	20.091	0.151	0.2028
15	Q_2, BN	1060	3.5	11.861	19.921	q	<0.3349
16	Q_2, BN	1060	4	18.085	19.919	–	>0.2483
7A	Q_2, BN	1080	1.8	0.872	1.856	–	>0.3896
7B	Q_2, BN	1080	1.8	1.143	3.503	–	>0.4789
8A	Q_2, BN	1080	1.5	0.619	2.358	q	<0.5332
8B	Q_2, BN	1080	1.5	0.574	3.505	q	<0.6467
10	Q_2, BN	1100	2	4.868	19.236	–	>0.5423
11	Q_2, BN	1100	1.5	4.000	20.204	–	>0.6023
12	Q_2, BN	1100	2.8	2.983	20.145	q	<0.6694
17	Q_2, BN	1130	2.5	2.502	20.156	q	<0.7072
18	Q_2, BN	1130	2	3.691	19.962	trace q	0.6186

Run-type abbreviations: Q_1, single quartz crystal; Q_2, fine-grained quartz; R, NaCl-only furnace; BN, BN+NaCl furnace (see text). Under quartz out, numerical entries give the weight of a single weighable quartz crystal, q indicates presence of fine-grained unweighable quartz, and a dash indicates quartz absent in run products. Uncertainty in reported SiO_2 mole fraction (X_s) is 0.042% relative (1σ), based on propagation of weighing errors.

with no loss of H_2O, as shown by repeated determinations of post-experiment H_2O mass balance in this laboratory (e.g., Newton and Manning, 2006, 2007; Tropper and Manning, 2007a,b).

Where SiO_2 mole fractions were greater than ~0.2, phase-assemblage bracketing (Q_2) experiments were conducted. This was because the Pt capsules could accommodate single quartz crystals of no more than ~20 mg, which required that H_2O mass be reduced if an experiment were to remain quartz saturated. However, at low H_2O contents the quartz crystals broke during experiments, yielding run products of recrystallized quartz aggregates that could not be collected and weighed with confidence. In addition, the run-product quartz crystals from high-solubility experiments were coated with a hard glassy matrix from which they could not be cleanly removed. These problems were circumvented using a bracketing method, in which the presence or absence of quartz in multiple isothermal, isobaric runs at different SiO_2 contents constrained the quartz saturation composition. Powdered quartz and H_2O from the same sources as in Q_1 runs were used in Q_2 experiments. The materials were loaded into capsules in the order H_2O then quartz powder, and sealed by arc welding as above.

All experiments were carried out in a piston-cylinder apparatus using 1.91 cm-diameter furnaces with graphite heater sleeves and NaCl pressure medium. The experiments spanned the temperature range 700–1130 °C (±3 °C). Temperature was measured and controlled automatically by calibrated, matched pairs of type C thermocouples. At the termination of a run, an experiment was quenched to <200 °C in <12 s by turning off the heating power.

Pressure in all experiments was 10±0.3 kbar. At temperatures less than 1000 °C, the NaCl pressure medium is solid and the pressure assemblies remained stable for indefinite periods. Above 1000 °C, NaCl melts in the immediate vicinity of the capsule and the assembly begins to deform. Eventually the graphite heater sleeve is breached by molten salt, leading to inhomogeneous temperature distributions and heater failure. For experiments above 1000 °C, discs of hot-pressed BN 0.4 cm in height were positioned above and below the sample capsule and the capsule was tightly packed in BN powder. The thermocouple tip remained in contact with the sample capsule. Because the BN was anticipated to be slightly less plastic than NaCl, we conducted a quartz solubility run at 950 °C with the BN-bearing assembly (Run 5, Table 1) to duplicate a run with only NaCl around the sample (Run 2, Table 1). The measured solubility of quartz in Run 5 was 5% lower than in Run 2, a difference that is larger than the precision observed in duplicate runs at similar conditions by Manning (1994). Using the pressure dependence of quartz solubility predicted by Manning (1994), the observed solubility difference translates to a pressure correction of −0.5 kbar for the BN-bearing furnace type. This correction was applied to all runs conducted at ≥1000 °C.

Crystals and H_2O were weighed before and after experiments on a Mettler M3 microbalance with a reproducibility of ±2 μg (1σ), as determined by repeated weighings of a standard. Propagation of weighing errors yields uncertainties in mole fractions of SiO_2 and H_2O (X_s and X_h, respectively) of 0.042% (1σ).

4. Results

Experimental results are given in Table 1. Results of weight-loss (Q_1) and bracketing (Q_2) experiments are consistent. In the bracketing runs, residual quartz was identified by optical and scanning-electron microscopy and occurred as rounded crystals of 50–100 μm diameter embedded in a chalky to glassy matrix in the quenched charges.

As illustrated in Fig. 3, the new determination of quartz solubility at 10 kbar, 750 °C, is consistent with previous work (Manning, 1994; Newton and Manning, 2000). In addition, data from this study extend the measurements along this isobar to 1130 °C. The results indicate that there is a large solubility increase at temperatures in the range 1000 to 1130 °C (Fig. 3).

The new data suggest a continuous rise in quartz solubility with increasing T, and point to a near-vertical tangent near 1080 °C (Fig. 3). As illustrated by Fig. 3, subcritical conditions would be indicated by a

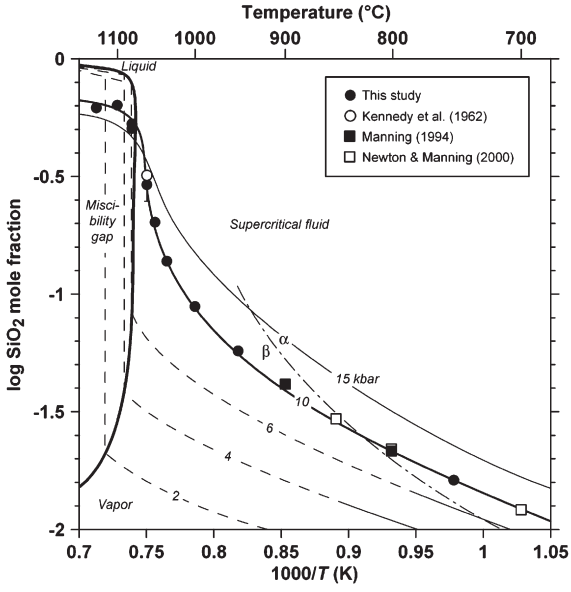

Fig. 3. Variation in quartz solubility in H_2O as a function of temperature. Bold loop is the liquid-vapor miscibility gap (Kennedy et al., 1962). Curves show solubility isobars: the 10 kbar isobar (solid) is based on data from this study, as well as from Kennedy et al. (1962, 9.5 kbar), Manning (1994) and Newton and Manning (2000). The 1σ errors and bracket widths in the data from the present study are smaller than the symbol size, except at 1050 °C, where solubility is given as the midpoint between bracketing experiments (shown by error bar). Light curves are approximate locations of other isobars, solid where based on well-constrained experimental determinations by Anderson and Burnham (1965), Manning (1994), Newton and Manning (2000) and Nakamura (1974), and dashed where less certain. The dash–dot curve is the α–β quartz inversion (Cohen and Klement, 1967). The near-vertical tangent of the 10-kbar isobar in the temperature interval 1050–1100 °C indicates the immediate proximity of critical mixing of fluids in equilibrium with quartz (i.e. a critical end point) at that pressure.

large increase in X_s over a very small T increase, whereas at P well in excess of the UCEP, tangents to the solubility curve would be relatively shallow at all T. Thus, the new data support the existence of a critical end point at 1080 °C, and at P only slightly lower than 10 kbar, as proposed originally by Kennedy et al. (1962). Further support for this conclusion lies in the topology of the solubility curve at >1080 °C. The polybaric three-phase envelope intersects the ordinate of Fig. 3 at one bar. Since the dry melting temperature increases with P (Jackson, 1976; Hudon et al., 2002), supercritical isobaric solubility curves must penetrate the three-phase loop in projection, with progressively shallower tangents as P rises. This is the topology exhibited by the new data (Fig. 3).

The bracketing experiments indicate that the composition of the critical fluid at 10 kbar lies between X_s of 0.47 and 0.57, again consistent with the conclusion of Kennedy et al. (1962) that the fluid composition at the UCEP is a nearly equimolar mixture. As T increases above 1000 °C at 10 kbar, and approaches the critical point at 1080 °C, the quenched and dried former fluid phase changes from a firm chalky texture to a translucent milky glass. This change takes place over no more than 30 °C. When the quenched fluid phase is glassy, the punctured capsules do not ooze excess fluid, which indicates that the H_2O content of quenched glass approaches 50 mole percent, probably as both structurally bound H_2O and as microvesicular water.

5. Discussion

5.1. Activity-concentration relations

The present experiments confirm a critical end point on the hydrous melting curve of quartz near 10 kbar, as proposed by Kennedy et al. (1962). The inferred critical temperature (T_c) is the same, but is based on experiments up to 50 times longer in the present work. In addition, the difficulty of recognizing a true melt phase based on the textures of quenched charges is circumvented by interpretation based on the shapes of the isobaric solubility curves, giving an unambiguous criterion of near-critical behavior, as shown in Fig. 3.

Although we present strong evidence for a UCEP at 1080 °C between 9.5 and 10 kbar, unresolved issues remain. For example, the nature of the speciation of solute silica near the critical point and how it may affect the onset of critical mixing is not clear. In addition, at subcritical conditions, there is no obvious reason for the nearly constant melting temperature with increasing P (Fig. 2), in spite of the very large compositional change of the melt approaching the UCEP. Equally puzzling is the composition of the critical fluid, which we have confirmed is nearly equimolar, as if there were some structural control mandating a quasi-regular fluid mixture.

The above questions may be addressed through derivation of activity-composition relations of SiO_2–H_2O mixtures. The present data on the isobaric compositional variation of a slightly supercritical quartz-saturated SiO_2–H_2O fluid with temperature can be combined with previous studies to obtain the activity-composition relations using two alternative approaches: first, by combination with lower-T experimental data on SiO_2 solubility in aqueous solutions; and second, by combination with data on the dry melting of quartz. The two approaches entail different standard states, and hence different activities and activity coefficients. Comparison of the results permits evaluation of the robustness of the conclusions drawn from the analysis.

5.1.1. Activities constrained by SiO_2 solubility in H_2O

Activities of total dissolved silica, $SiO_{2,aq}$, and H_2O can be calculated at 10 kbar at quartz saturation and near-critical conditions by combining data from the present study with previous work on silica solubility at the same P, but lower T. Quartz solubility in H_2O is described by Eq. (4). At 10 kbar, $SiO_{2,aq}$ concentration in equilibrium with quartz increases with T to ~2 molal at 900 °C (Manning, 1994). This concentration is sufficiently dilute that $SiO_{2,aq}$ in quartz-saturated H_2O – and all undersaturated solutions – exists almost completely as $Si(OH)_4$ monomers and $Si_2O(OH)_6$ dimers (Newton and Manning, 2002, 2003; Zotov and Keppler, 2002). A convenient standard state for $SiO_{2,aq}$ in the presence of multiple species is the hypothetical solution with unit mole fraction of monomers (X_m), referred to infinite dilution. Thus, the activity of $SiO_{2,aq}$ on this solute standard state, $a_{s,s}$, is related to $\gamma_{s,s}$, and X_m as

$$a_{s,s} = \gamma_{s,s} X_s = X_m \tag{6}$$

Using a standard state for minerals (and H_2O) of unit activity of the pure phase at any P and T, the standard molal Gibbs energy change of Eq. (4) (ΔG_4°) is thus

$$\ln a_{s,s}^{Q} = \frac{-\Delta G_4^\circ}{RT} \tag{7}$$

where $a_{s,s}^{Q}$ refers to $SiO_{2,aq}$ activity at quartz saturation, R is the gas constant, and T is in Kelvin. Evaluation of $SiO_{2,aq}$ and H_2O activity-concentration relations therefore requires values of ΔG_4° at the conditions of the present study.

Values of ΔG_4° were calculated at 700–900 °C using data of Newton and Manning (2002, their Table 3), and are plotted in Fig. 4. A least-squares fit to the data gives

$$\Delta G_4^\circ = 66.84 - 1.689 \times 10^4/T - 6.520 \times 10^6/T^2 \tag{8}$$

(R^2=0.998), which permits modest extrapolation to the conditions of the present study.

Combination of Eqs. (6)–(8) allows calculation of $a_{s,s}^{Q}$ and $\gamma_{s,s}^{Q}$ for our experimental conditions (Supplementary data, Fig. 5). Fig. 5 illustrates that the activity of $SiO_{2,aq}$ is nearly constant over a broad range of X_s in the narrow T interval within ~50 °C of the critical temperature. This is the expected behavior of near-critical solutions.

The activity of H_2O in near-critical quartz-saturated H_2O–SiO_2 solutions can be derived from the experimental data if it is assumed that $a_{s,s}$ is independent of temperature within 50 °C of the critical temperature, as suggested by the data in Fig. 5. That is, we assume that isothermal activity–concentration relations at $T=T_c$=1080 °C are approximated by the very slightly polythermal relations at ±50 °C

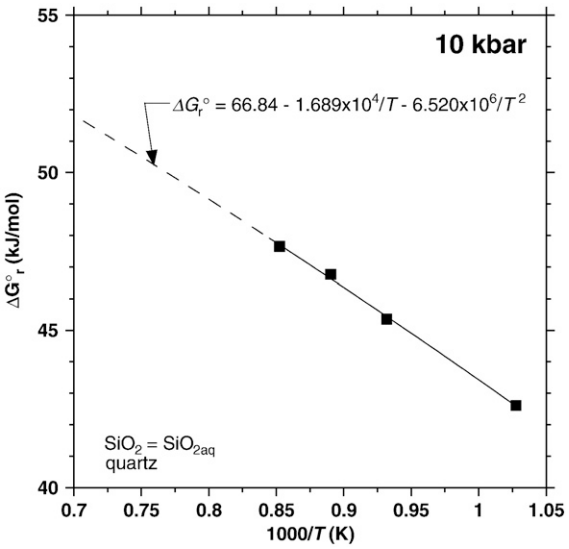

Fig. 4. Standard Gibbs free energy at 10 kbar of the quartz dissolution reaction (Eq. (4), text). Filled squares calculated using data in Newton and Manning (2002). The line is a least squares regression to the data (Eq. (8)), dashed where extrapolated.

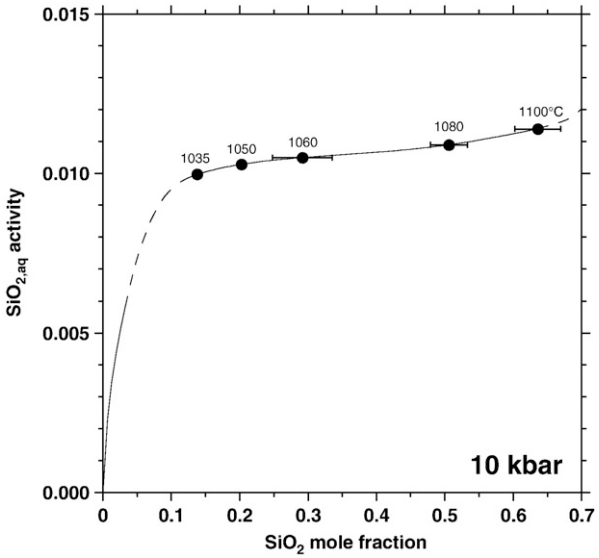

Fig. 5. Activity–composition relations of SiO_2 relative to the "solute" standard state (Eq. (6)) at 10 kbar in the nearly isothermal range 1030–1100 °C. Filled circles show values calculated from measured compositions at quartz saturation using equations and data of Newton and Manning (2002). The nearly constant activity of SiO_2 despite 3-fold increase in SiO_2 mole fraction indicates the existence of a critical end point near 10 kbar and in the range 1030–1100 °C. The curve is a cubic spline to the data of this study and calculated $a_{s,s}$ values at 1080 °C and $X_s \leq 0.034$ (≤2 molal SiO_2; see text); the spline is dashed where interpolated between X_s of 0.034 and 0.139, which corresponds to the compositional constraint derived from the 1035 °C experiment. The activity–composition relations derived from the cubic spline function were used to model mixing relations at the critical temperature (see text).

quartz saturation. With this assumption, integration of the Gibbs–Duhem relation at constant P and T gives γ_h as a function of X_s and $\gamma_{s,s}$:

$$\ln\gamma_h = -\int_0^{\ln\gamma_{s,s}} \frac{X_s}{1-X_s} d\ln\gamma_{s,s} \tag{9}$$

Data for X_s^Q and $\gamma_{s,s}^Q$ from 1035–1080 °C (Supplementary data) were fitted to an exponential function to yield:

$$\ln\gamma_h = 0.00266\left[\exp\left(1.539\ln\gamma_{s,s}\right)-1\right] \tag{10}$$

which leads to a_h via

$$a_h = (1-X_s)\gamma_h \tag{11}$$

The derived H_2O activity–concentration relations are given in the supplementary data table and shown in Fig. 6. As with $a_{s,s}^Q$, the model predicts nearly constant a_h at near-critical conditions over a broad range of composition. More importantly, values of a_h are remarkably high; the results suggest that $a_h > 0.9$ up to silica mole fractions of 0.6.

5.1.2. Activities constrained by dry quartz melting

An alternative, independent approach to the determination of activity–concentration relations is to utilize the depression of the melting point of quartz by H_2O (cf., Kennedy et al., 1962). Here, the standard state for SiO_2 is taken to be unit activity of pure molten silica ($SiO_{2,liq}$), while that for quartz and H_2O remains unit activity of the pure phase. Jackson (1976) gives an equilibrium temperature of 1840 °C for dry quartz melting,

$$\underset{\text{quartz}}{SiO_2} = SiO_{2,liq} \tag{12}$$

at 10 kbar Hudon et al. (2002) determined a slightly higher temperature of 1900±20 °C, but this small temperature difference does not materially affect the calculations. The standard Gibbs free energy of metastable melting at 10 kbar and any lower temperature is given, to a good approximation, by:

$$\Delta G_{12}^{\circ} = (1840-T)\Delta S_{12}^{\circ} \tag{13}$$

with T in °C, where ΔS_{12}^{o} is a mean value of the entropy of melting. Richet et al. (1982) give a calorimetric one-bar value of ΔS_{12}^{o} of 5.53 J/mol K at their preferred metastable melting point of quartz of 1427 °C. This value is used to calculate SiO_2 activity from:

$$\ln a_{s,l} = \frac{-\Delta G_{12}^{\circ}}{RT} \tag{14}$$

where $a_{s,l}$ denotes activity of silica calculated on the "liquid" standard state. Eq. (14) gives calculated activities at 1035–1100 °C, which are shown in Fig. 6.

The value of ΔS_{12}° should be relatively insensitive to P along the melting curve of quartz up to 10 kbar, so that the one-bar value may be considered representative. However, if the metastable melting point of quartz at one bar is actually as low as 1427 °C, as proposed by Richet et al. (1982), the Clausius–Clapeyron equation mandates that the volume change of melting would be >100%, which is implausible. Navrotsky (1994, p. 314) suggests a melting point that is 200 °C higher. If the Richet et al. (1982) value of 6.2 J/mol K for ΔS_{12}° at 1627 °C is used instead of 5.53 J/mol K, only slightly lower values of the calculated SiO_2 activities result. In view of the uncertainties in the calculation, the value of 5.53 is retained.

Calculated values of $a_{s,l}^Q$ at 10 kbar are very nearly constant over the roughly isothermal range of 1050–1100 °C (Supplementary data, Fig. 6), as would be expected of a near-critical isobar. By again making the assumption that isothermal activity–concentration relations at $T = T-=1080$ °C are approximated by the polythermal, quartz–saturated

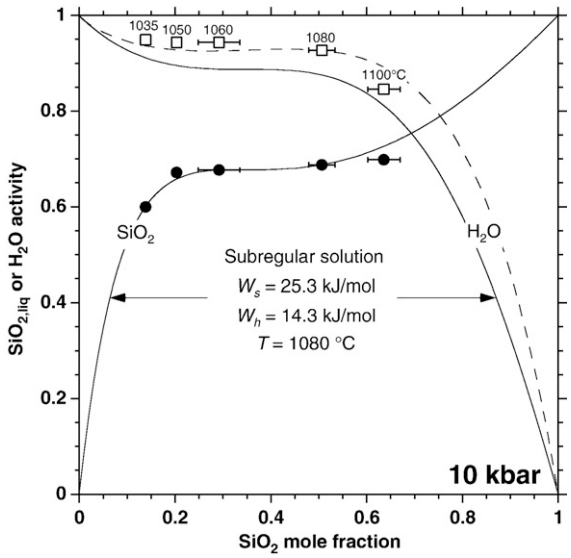

Fig. 6. Activity–concentration relation of SiO_2 and H_2O at 10 kbar in the nearly isothermal range 1035–1100 °C. The filled circles were calculated on the "liquid" standard state from the depression of the melting point of quartz in the presence of H_2O. The solid curves show results of fitting to a subregular solution model with a critical point of 1080 °C, which gave interchange energies of $W_s = 25.3$ and $W_h = 14.3$ kJ/mol (see text). The close adherence of the experimental points to the model critical activity–concentration curve confirms the existence of a critical end point close to the assumed P–T conditions. Open squares show H_2O activity calculated from the present data set by Gibbs–Duhem inversion of $a_{s,s}$ values (Fig. 5); the dashed curve gives H_2O activity calculated from Eq. (11). The data are in good agreement with the H_2O activities predicted by subregular theory.

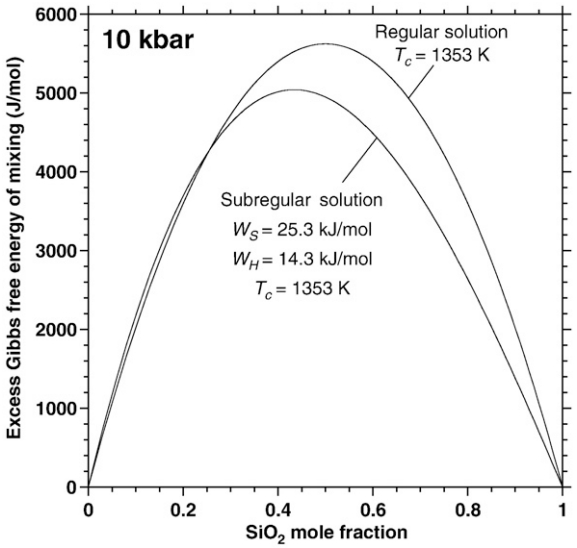

Fig. 7. Excess Gibbs free energy of mixing in SiO_2–H_2O fluids at 1080 °C and 10 kbar as modeled by a subregular solution, compared with a regular solution with critical temperature of 1080 °C.

relations at 1050–1100 °C, the near-critical data of the present study may be fitted to a subregular solution model, in which

$$\ln a_{s,l} = \ln X_s + \frac{(1-X_s)^2(W_s + 2X_s(W_h - W_s))}{RT_c} \quad (15)$$

where W_s and W_h are respectively the interchange energies for $SiO_{2,liq}$ and H_2O, and T_c is taken to be 1353 K. Least squares fitting, subject to the assumption that the system is not subcritical (i.e., $(\partial \ln a_s/\partial \ln X_s)_{P,T} \geq 0$), yields W_s = 25.3 kJ/mol and W_h = 14.3 kJ/mol (Fig. 6). These parameters return a critical composition of X_s = 0.35 at 1080 °C. If 1900 °C were used for the quartz melting temperature (Hudon et al., 2002), Wh would be 13.0 kJ/mol and Ws would be unchanged.

The interchange energies derived above allow the activity of H_2O to be calculated from

$$\ln a_h = \ln(1-X_s) + \frac{X_s^2(W_h + 2(1-X_s)(W_s - W_h))}{RT_c} \quad (16)$$

Fig. 6 illustrates that the variation in a_h with X_s yields quite good agreement with values derived from extension of the solubility model of Newton and Manning (2002). If a characteristic ΔS^o_{12} of 6.2 J/mol K is used in place of 5.53 J/mol K, the agreement would be even better.

Fig. 7 shows that the derived subregular excess Gibbs free energy of mixing of SiO_2 and H_2O at 10 kbar and 1080 °C is quite close to that of a simple, symmetric solution of the same critical temperature. It is surprising that mixing of SiO_2 and H_2O at P and T near the upper critical end point nearly corresponds to a regular solution, given the expected complexities of polymerization and hydration state of solute complexes which must occur in the concentrated SiO_2 region. This observation prompted an analysis of speciation of solute silica at the critical temperature.

5.2. Speciation of $SiO_{2,aq}$ at the critical temperature

The variation in species abundance with composition at T_c = 1080 °C can be derived by combining the monomer-dimer mixing model of Newton and Manning (2002) with results of the present study. Newton and Manning (2002) found that at ≤2 molal, or $X_s \leq 0.034$, $SiO_{2,aq}$ could be successfully modeled as a mixture solely of monomers and dimers. Assuming that this compositional limit holds at 1080 °C, we derived an extrapolated value of K_1 = 390 from the data of Newton and Manning (2002). This allows calculation of $\gamma_{s,s}$ at 1080 °C at $X_s \leq 0.034$ by rearrangement of Eq. (3). The resulting values of $a_{s,s}$, (Eq. (6)) are shown in Fig. 5. A cubic spline routine was then used to derive the functional form of the activity–composition curve relating the data at 1035–1100 °C to the extrapolated $a_{s,s}$ values at $X_s \leq 0.034$ (Fig. 5), which gives the X_m directly (Eq. (6)). This in turn allows solution of Eq. (2) for dimer mole fraction (X_d). Mass balance dictates that the fraction of SiO_2 residing in species other than monomers and dimers, which must be higher oligomers, is simply the difference between X_s and the sum $X_m/X_s + 2X_d/X_s$.

Fig. 8 shows the variation in the populations of monomers, dimers and higher oligomers at 1080 °C, 10 kbar. The activity of silica relative to the monomeric species, which is taken to be the molar concentration of the latter, decreases dramatically with SiO_2 concentration, its place being taken by the dimer. However, as a consequence of Eq. (2), the dimer concentration passes through a maximum and then begins to decline, still at low X_s (Fig. 8). The balance of the solute silica at high concentrations must be some unspecified distribution of higher oligomers. At 1080 °C, quartz saturation is attained at the critical composition. This is the only fluid composition which can be in equilibrium with quartz in Fig. 8. Higher oligomers account for nearly 80% of the silica in solution.

6. Interpretations

There are three important features of the slightly supercritical, isobaric activity–concentration relations shown in Figs. 5 and 6. First, there is a very broad range of X_s where SiO_2 activity is nearly constant. In addition, the results point to a sudden upswing of SiO_2 activity at $X_s > 0.6$. Finally, both approaches to the calculation of activity–concentration relations yield very high and nearly constant H_2O activity, persisting to surprisingly high X_s. It is this last feature which explains the fact that the H_2O content of the hydrous melt in equilibrium with quartz increases dramatically with pressure along the melting curve as the UCEP is approached, while the melting temperature remains nearly constant (Fig. 2). When the H_2O mole fraction reaches 0.5, the siliceous fluid seems energetically inert to

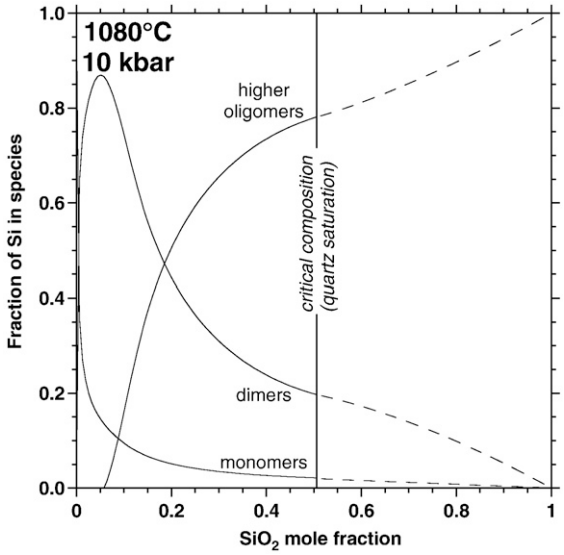

Fig. 8. Distribution of polymeric silica species at the upper critical pressure and temperature (10 kbar, 1080 °C) in the system SiO_2–H_2O, determined from Eqs. (1)–(7), text. All polymers higher than dimer are lumped together as "higher oligomers". Quartz can be in equilibrium with a critical fluid only at the critical composition. Solid curves are for compositions undersaturated with respect to quartz. Dashed curves are for metastable oversaturation in SiO_2.

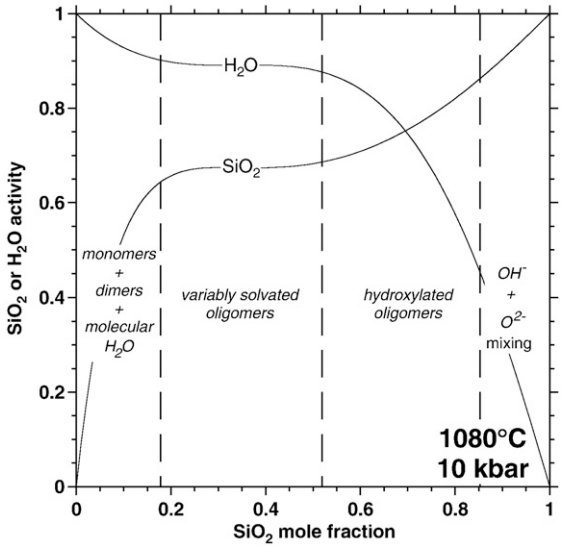

Fig. 9. Interpretation of the slopes of the SiO_2 and H_2O activity functions at the critical temperature (~1080 °C) and critical pressure (~10 kbar). In the siliceous melt region with relative low H_2O, the dissolved H_2O is almost entirely hydroxyl. The large energy of this kind of bonding accounts for the rapid depression of the melting temperatures of the silica polymorphs at low pressures (see Fig. 1). As H_2O concentration approaches a composition of stoichiometry H_2SiO_3, the OH^- is saturated. Further hydration is possible via hydrogen-bonded molecular H_2O. It is possible that ring-structure solutes of composition $Si_nO_n(OH)_{2n}$, account for special stability of a critical fluid.

further H_2O input, until very high H_2O contents are reached in supercritical fluids.

The activity–concentration behavior of SiO_2-rich fluids may be interpreted in terms of partitioning of H_2O between hydroxyl and molecular H_2O, in the manner envisioned by Burnham and Davis (1974) for hydrous melting of albite, $NaAlSi_3O_8$. In that study, $NaAlSi_3O_8$ and H_2O activities were derived from measured melt compositions and partial molal volumes measured over ranges of temperature, pressure, and composition. Two discrete activity–composition regions were noted at fixed T and P: one for H_2O concentrations up to 50 mol%, in which the energetic effects of H_2O solution are large, with H_2O activity proportional to the square of H_2O mole fraction, and a more hydrous region in which H_2O activity rises rapidly with additional H_2O input. The X_h^2 behavior was interpreted by Burnham and Davis (1974) as the effect of dissociation of H_2O to form 2 OH^-, aided energetically by the formation of charge-balancing Na^+ ions. This behavior persists until the Na becomes exhausted at $X_h = 0.50$. Additional H_2O may still enter the melt as molecular H_2O, but with diminished energetic effects.

The activity–composition relations in the system SiO_2–H_2O in the near-critical region seem analogous to those in the system $NaAlSi_3O_8$–H_2O. In the absence of the exchangeable cation Na^+, it is not certain whether or not the H_2O as hydroxyl at low concentration in silica-rich fluids is fully dissociated. If dissociation is incomplete, the two OH^- created by dissolved H_2O may remain locally associated in charge-balanced units, and the H_2O activity would be expected to be directly proportional to the concentration, rather than to the square of the concentration. The present data are not sufficient to decide on this point.

In the present interpretation, the silica-rich fluid near the critical end point T and P can reasonably be modeled as a "lattice gas" (Kennedy et al., 1962), with O_2^- mixing with OH^- in a quasi-ideal fashion. This effect appears to saturate near 40 mol% H_2O, as OH^- substitution terminates in solutes of overall stoichiometry H_2SiO_3. Such solutes may be in reality ring structures of composition $Si_nO_n(OH)_{2n}$. A fluid composed dominantly of such rings may be a very stable phase with rings hydrogen-bonded to adjacent rings in an optimal way. Higher H_2O concentrations are possible in a ring-dominated fluid as hydrogen-bonding of H_2O molecules to the rings replaces self-bonding of rings. Hydrogen-bonded H_2O would have high fugacity and activity near unity, approaching the partial molal free energy of a pure H_2O fluid at the same P and T, similar to the behavior of molecular H_2O in structural cavities in zeolites or cordierite (Newton and Wood, 1980). The hydrogen-bonding effect saturates below about $X_s = 0.2$, as all of the O^{2-} and OH^- of the higher oligomers are saturated with hydrogen bonds. Further increase of H_2O concentration results in dissociation of higher oligomers into dimers and monomers, which are stabilized by their greater mixing capability. SiO_2 activity remains high in near-critical fluids over a broad range of compositions at $X_s < 0.5$ because the mole fraction of higher oligomers remains nearly constant as incoming H_2O molecules are hydrogen-bonded to them, rather than adding to a diluting species. Oligomerization, coupled with hydrogen bonding, is thus envisioned as a convergence or cooperation mechanism by which full miscibility is achieved. The several characteristic mixing regions in supercritical SiO_2–H_2O fluids are diagrammed in Fig. 9.

The foregoing conjectures may be tested with additional experimental data of various kinds. These include accurate determination of supercritical isobars of quartz saturation, searching for systematics of SiO_2 activity in the manner of Burnham and Davis (1974) in the system $NaAlSi_3O_8$–H_2O, determination of the solubility of quartz in CO_2–H_2O mixtures over ranges of P and T in order to investigate the extent of hydrogen bonding in the manner of Walther and Orville (1983), and Raman spectroscopy in the externally heated diamond pressure cell at the highest possible SiO_2 concentrations, searching for evidence of the ring species and higher polymers.

Acknowledgements

Wayne Dollase alerted the authors to the possibly important role of hydrogen bonding in high P-T, SiO_2–H_2O fluids. He, David Dolejs, and Jon Hunt provided very stimulating discussions. We thank J. Mavrogenes and A. Hack for helpful reviews of the manuscript. This research was supported by U.S. National Science Foundation grant EAR-0711521.

Appendix A. Supplementary data

Supplementary data associated with this article can be found, in the online version, at doi:10.1016/j.epsl.2008.07.028.

References

Anderson, G.M., Burnham, C.W., 1965. The solubility of quartz in supercritical water. Am. J. Sci. 263, 494–511.
Audétat, A., Keppler, H., 2004. Viscosity of fluids in subduction zones. Science 303, 513–516.
Bureau, H., Keppler, H., 1999. Complete miscibility between silicate melts and hydrous fluids in the upper mantle: experimental evidence and geochemical implications. Earth Planet. Sci. Lett. 165, 187–196.
Burnham, C.W., Davis, N.F., 1974. The role of H_2O in silicate melts: II. Thermodynamic and phase relations in the system $NaAlSi_3O_8$–H_2O to 10 kilobars, 700°–1100 °C. Am. J. Sci. 274, 902–940.
Cohen, L.H., Klement Jr., W., 1967. High–low quartz inversion: determinations to 35 kilobars. J. Geophys. Res. 72, 4245–4251.
Gerya, T.V., Maresch, W.V., Burchard, M., Zakhartchouk, V., Doltsinis, N.L., Fockenberg, T., 2005. Thermodynamic modeling of solubility and speciation of silica in H_2O–SiO_2 fluid up 1300 °C and 20 kbar based on the chain reaction formalism. Eur. J. Mineral. 17, 269–283.
Guggenheim, E.A., 1952. Mixtures. Clarendon Press, Oxford.
Hack, A.C., Thompson, A.B., Aerts, M., 2007a. Phase relations involving hydrous silicate melts, aqueous fluids, and minerals. Rev. Mineral. Geochem. 65, 129–185.
Hack, A.C., Hermann, J., Mavrogenes, J.A., 2007b. Mineral solubility and hydrous melting relations in the deep earth: analysis of some binary A-H_2O system pressure–temperature-composition topologies. Am. J. Sci 307, 833–855.
Hermann, J., Spandler, C.J., 2008. Sediment melts at sub-arc depths. J. Petrol. 49, 717–740.
Hudon, P., Jung, I.H., Baker, D.R., 2002. Melting of β-quartz up to 2.0 GPa and thermodynamic optimization of the silica liquidus up to 6.0 GPa. Phys. Earth Planet. Int 130, 159–174.
Jackson, I., 1976. Melting of silica isotypes SiO_2, BeF_2 and GeO_2 at elevated pressures. Phys. Earth Planet. Inter. 8, 277–281.

Kennedy, G.C., 1950. A portion of the system silica–water. Econ. Geol. 45, 629–653.
Kennedy, G.C., Wasserberg, G.J., Heard, H.C., Newton, R.C., 1962. The upper three-phase region in the system SiO_2–H_2O. Am. J. Sci. 260, 501–521.
Kessel, R., Ulmer, P., Pettke, T., Schmidt, M.W., Thompson, A.B., 2005a. The water-basalt system at 4 to 6 GPa: phase relations and second critical end point in a K-free ecolgite at 700 to 1400 °C. Earth Planet. Sci. Lett. 237, 873–892.
Kessel, R., Schmidt, M.W., Ulmer, P., Pettke, T., 2005b. Trace element signature of subduction-zone fluids, melts and supercritical fluids at 120–180 km depth. Nature 437, 724–727.
Manning, C.E., 1994. The solubility of quartz in H_2O in the lower crust and upper mantle. Geochim. Cosmochim. Acta 58, 4831–4839.
Manning, C.E., 2004. The chemistry of subduction-zone fluids. Earth Planet. Sci. Lett. 223, 1–16.
Mibe, K., Kanzaki, M., Kawamoto, T., Matsukage, K.N., Fei, Y.W., Ono, S., 2007. Second critical endpoint in the peridotite-H_2O system. J. Geophys. Res. 112 Art. no. B03201.
Morey, G.W., Hesselgesser, J.M., 1951. The solubility of some minerals in superheated steam at high pressures. Econ. Geol. 46, 821–835.
Mysen, B.O., 1998. Interaction between aqueous fluid and silicate melt in the pressure and temperature regime of the Earth's crust and upper mantle. Neues Jb. Miner. Abh. 172, 225–251.
Nakamura, Y., 1974. The system SiO_2–H_2O–H_2 at 15 kbar. Carn. Inst. Wash. Yearbook 73, 259–263.
Navrotsky, A., 1994. Thermochemistry of crystalline and amorphous silica. Rev. Mineral. 29, 309–329.
Newton, R.C., Manning, C.E., 2000. Quartz solubility in H_2O–NaCl and H_2O–CO_2 solutions at deep crust–upper mantle pressures and temperatures: 2–15 kbar and 500–900 °C. Geochim. Cosmochim. Acta 64, 2993–3005.
Newton, R.C., Manning, C.E., 2002. Solubility of enstatite + forsterite in H_2O at deep crust/upper mantle conditions: 4 to 15 kbar and 700 to 900 °C. Geochim. Cosmochim. Acta 66, 4165–4176.
Newton, R.C., Manning, C.E., 2003. Activity coefficient and polymerization of aqueous silica at 800 °C, 12 kbar, from solubility measurements on SiO_2-buffering mineral assemblages. Contrib. Mineral. Petrol. 146, 135–143.
Newton, R.C., Manning, C.E., 2006. Solubilities of corundum, wollastonite and quartz in H_2O–NaCl solutions at 800 °C and 10 kbar: Interaction of simple minerals with brines at high pressure and temperature. Geochim. Cosmochim. Acta 70, 5571–5582.
Newton, R.C., Manning, C.E., 2007. Solubility of grossular, $Ca_3Al_2Si_3O_{12}$, in H_2O–NaCl solutions at 800 °C and 10 kbar, and the stabililty of garnet in the system $CaSiO_3$–Al_2O_3–NaCl–H_2O at 800 °C and 10 kbar. Geochim. Cosmochim. Acta 71, 5191–5202.
Newton, R.C., Wood, B.J., 1980. Thermodynamics of water in cordierite and some petrologic consequences of cordierite as a hydrous phase. Contrib. Mineral. Petrol. 68, 391–405.
Richet, P., Bottinga, Y., Danielou, L., Petitet, J.P., Tequi, C., 1982. Thermodynamic properties of quartz, cristobalite and amorphous silica: drop calorimetry measurements between 1000 and 1800 K and a review from 0 to 2000 K. Geochim. Cosmochim. Acta 46, 2639–2658.
Shen, A., Keppler, H., 1997. Direct observation of complete miscibility in the albite-H_2O system. Nature 385, 710–712.
Sommerfeld, R.A., 1967. Quartz solution reaction: 400–500 °C, 1000 bars. J. Geophys. Res. 72, 4253–4257.
Sowerby, J.R., Keppler, H., 2002. The effect of fluorine, boron and excess sodium on the critical curve in the albite-H_2O system, contrib. Mineral. Petrol. 143, 32–37.
Stalder, R., Ulmer, P., Thompson, A.B., Günther, D., 2000. Experimental approach to constrain second critical end points in fluid/silicate systems: near-solidus fluids and melts in the system albite-H_2O. Am. Mineral. 85, 68–77.
Stewart, D.B., 1967. Four-phase curve in the system $CaAl_2Si_2O_8$–SiO_2–H_2O between 1 and 10 kbar. Schweiz. Miner. Petrog. 47, 35–59.
Tropper, P., Manning, C.E., 2007a. The solubility of corundum in H_2O at high pressure and temperatgure and its implications for Al mobility in the deep crust and upper mantle. Chem. Geol. 240, 54–60.
Tropper, P., Manning, C.E., 2007b. The solubility of fluorite in H_2O and H_2O–NaCl at high pressure and temperature. Chem. Geol. 242, 299–306.
Walther, J.V., Orville, P.M., 1983. The extraction-quench technique for determination of the thermodynamic properties of solute complexes; applications to quartz solubility in fluid mixtures. Am. Mineral. 68, 731–741.
Wasserburg, J.G., 1957. The effects of H_2O in silicate systems. J. Geol. 65, 15–23.
Weill, D.F., Fyfe, W.S., 1964. The solubility of quartz in H_2O in the range 1000–4000 bars and 400–500 °C. Geochim. Cosmochim. Acta 28, 1243–1255.
Wyart, J., Sabatier, G., 1955. Nouvelles mesures de la solubilité du quartz, de la tridymite, et de la cristobalite dans l'eau sous pressions au-dessus de la température critique. Acad. Sci. Comptes Rend. 240, 1905–1907.
Zhang, Y.-G., Frantz, J.D., 2000. Enstatite–forsterite–water equilibria at elevated temperatures and pressures. Am. Mineral. 85, 918–925.
Zotov, N., Keppler, H., 2000. In-situ Raman spectra of dissolved silica species in aqueous fluids to 900 °C and 14 kbar. Am. Mineral. 85, 600–604.
Zotov, N., Keppler, H., 2002. Silica speciation in aqueous fluids at high pressures and temperatures. Chem. Geol. 184, 71–82.